Mon. Not. R. Astron. Soc. **337,** 133–146 (2002)

A deep *UBVRI* CCD photometric study of the open clusters Tr 1 and Be 11

R. K. S. Yadav[1]★ and Ram Sagar[1,2]★

[1]*State Observatory, Manora Peak Nainital 263129, India*
[2]*Indian Institute of Astrophysics, Bangalore 560034, India*

Accepted 2002 July 19. Received 2002 July 12; in original form 2002 March 21

ABSTRACT

We present deep *UBVRI* charge-coupled device (CCD) photometry for the young open star clusters Tr 1 and Be 11. The CCD data for Be 11 are obtained for the first time. The sample consists of ∼1500 stars reaching down to $V \sim 21$ mag. Analysis of the radial distribution of the stellar surface density indicates that radius values for Tr 1 and Be 11 are 2.3 and 1.5 pc, respectively. The interstellar extinction across the face of the imaged clusters region seems to be non-uniform with a mean value of $E(B-V) = 0.60 \pm 0.05$ and 0.95 ± 0.05 mag for Tr 1 and Be 11, respectively. A random positional variation of $E(B-V)$ is present in both the clusters. In the cluster Be 11, the reason for the random positional variation may be the apparent association of the H II region (S 213). The 2MASS *JHK* data in combination with the optical data in the cluster Be 11 yield $E(J-K) = 0.40 \pm 0.20$ mag and $E(V-K) = 2.20 \pm 0.20$ mag. Colour excess diagrams indicate a normal interstellar extinction law in the direction of the cluster Be 11.

The distances to Tr 1 and Be 11 are estimated as 2.6 ± 0.10 and 2.2 ± 0.10 kpc, respectively, while the theoretical stellar evolutionary isochrones fitted to the bright cluster members indicate that the clusters Tr 1 and Be 11 are 40 ± 10 and 110 ± 10 Myr old, respectively. The mass functions corrected for both field star contamination and data incompleteness are derived for both clusters. The slopes 1.50 ± 0.40 and 1.22 ± 0.24 for Tr 1 and Be 11, respectively, are in agreement with the Salpeter value. Observed mass segregations in both clusters may be the result of dynamical evolutions or the imprint of star formation processes or both.

Key words: Hertzsprung–Russell (HR) diagram – stars: luminosity function, mass function – open clusters and associations: individual: Tr 1 – open clusters and associations: individual: Be 11 – galaxies: star clusters.

1 INTRODUCTION

Young open star clusters in a galaxy provide valuable information concerning star formation processes and are key objects for the galactic structure and evolution. For such studies, a knowledge of cluster parameters such as distance, age, reddening and stellar content is required, which can be derived from the colour–magnitude (CM) and colour–colour (CC) diagrams of star clusters. In addition to this, the distribution of stellar masses at the time of cluster formation is of fundamental importance to the analysis of the evolution of galaxies. The initial mass function (IMF) also plays an important role in understanding the early dynamical evolution of star clusters, because it is a fossil record of the very complex process of star formation and provides an important link between the easily observable population of luminous stars in a stellar system and the fainter, but dynamically more important, low-mass stars. Another related problem is the mass segregation in star clusters in which massive stars are more concentrated towards the cluster centre compared with low-mass stars. It is not clear whether the mass segregation observed in several open clusters is a result of dynamical evolution or an imprint of the star formation process itself (cf. Sagar et al. 1988; Sagar 2002 and references therein). Thus, one can say that the young open star clusters are the laboratories in a galaxy for providing answers to many current questions of astrophysics.

In light of the above discussions, we performed multicolour deep charge-coupled device (CCD) stellar photometry in two young open star clusters, namely Trumpler 1 (Tr 1) and Berkeley 11 (Be 11). The CCD *UBVRI* observations of Be 11 are presented for the first time. The relevant prior information (taken from Mermilliod 1995) of a cluster is given in Table 1. These clusters are relatively compact objects with angular radii of less than *3* arcmin. Previous studies, observations and data reductions are described in the next sections.

★E-mail: rkant@upso.ernet.in (RKSY); sagar@upso.ernet.in (RS)

Table 1. General information concerning the clusters under study, taken from Mermilliod (1995).

Cluster	IAU	OCL	l (deg)	b (deg)	Trumpler class	Radius (arcmin)	Distance (kpc)	$E(B-V)$ (mag)	log(age) (yr)
Trumpler 1	C0132 + 610	328	128.22	−1.14	II 2p	1.5	2.6	0.58	7.5
Berkeley 11	C0417 + 448	404	157.08	−3.65	II 2m	2.5	2.2	0.95	7.7

The interstellar extinction, other photometric results, luminosity function (LF), mass function and mass segregation are described in the subsequent sections.

2 PREVIOUS STUDIES

Trumpler 1. It is an extremely concentrated galactic open star cluster in Cassiopeia, lying at the outer edge of the Perseus spiral arm. Oja (1966) carried out a proper motion study. *UBV* photoelectric photometry for 43 bright stars was presented by Joshi & Sagar (1977), while Phelps & Janes (1994) published *UBV* CCD photometry ($V \sim 18$ mag). McCuskey & Houk (1964) studied this cluster photographically in the *UBV* system, while Steppe (1974) presented three-colour RGU photographic photometry. All of these studies indicate that reddening across the cluster is uniform with $E(B-V) = 0.61$ mag, a distance estimate of 2630 pc and the age seems to be ∼27 Myr.

Berkeley 11. It is a distant neglected compact young open cluster, apparently associated with the faint H II region S 213. Only *UBV* photoelectric photometry of 24 bright stars has been carried out by Jackson, Fitzgerald & Moffat (1980). On the basis of this study, they found that this cluster has members of the earliest photometric type ∼b4 and is thus an extreme Population I object. They also found a reddening of $E(B-V) = 0.95 \pm 0.06$ mag, distance $d = 2.2 \pm 0.2$ kpc and the age of the cluster as 3×10^7 yr.

3 OBSERVATIONAL DATA

The optical and near-infrared (near-IR) *JHK* data used in the present study are described in the following subsections.

3.1 Optical observations and data reductions

The *UBV* Johnson and *RI* Cousins observations were obtained, using a 2K × 2K CCD system at the $f/13$ Cassegrain focus of the Sampurnanand 104-cm telescope of the State Observatory, Nainital during 2000 November. Details of the observations are given in Table 2. Each pixel of 2048 × 2048 size CCD corresponds to a square of size 0.36 arcsec on the sky. In order to improve theS/N ratio, the observations were taken in a binning mode with 2 × 2 pixels. The entire chip covers a field of 12.3 × 12.3 arcmin^2, though because of the smaller filter sizes we could image only a ∼8.6 × 8.6 arcmin^2 region. The read-out noise for the system is 5.3 e$^-$ with a gain of 10 e$^-$ ADU^{-1}. In each passband, only one short but two to three deep exposures were taken for the cluster region so that accurate photometric measurements could be obtained for faint stars. To remove field star contamination, we also observed field regions in the *UBV* $(RI)_C$ passband situated ∼15-arcmin south for both clusters. Fig. 1 show the identification maps of imaged cluster and field regions of Tr 1 and Be 11. For calibration, we observed 11 Landolt (1992) standard stars covering a range in brightness ($11.0 < V < 15.0$) as well as in colour [$0.16 < (V-I) < 2.08$]. Flat-field exposures ranging from 20 to 60 s in each filter were made on the twilight sky. A number of biases were also taken during the observing runs.

The CCD data frames were reduced using computing facilities available at the State Observatory, Nainital. Initial processing of the data frames were done in the usual manner using the IRAF data reduction package. Different cleaned frames of the same field in the same filter were co-added. Photometry of co-added frames was carried out using the DAOPHOT software (Stetson 1987). The point spread function (PSF) was obtained for each frame using several

Table 2. Log of CCD observations. *N* denotes the number of stars measured in different passbands.

Region	Filter	Exposure time (s)	Date	*N*
Trumpler 1 – cluster	*U*	1800 × 2, 300 × 1	2000 November 19, 20	524
$\alpha_{2000} = 01^h35^m40^s$	*B*	1200 × 3, 240 × 1	,,	1283
$\delta_{2000} = +61^d17'20''$	*V*	900 × 3, 120 × 1	,,	1451
	R	480 × 3, 60 × 1	,,	1630
	I	240 × 3, 60 × 1	,,	1710
Trumpler 1 – field	*U*	1200 × 1	2000 November 20, 21	350
$\alpha_{2000} = 01^h35^m40^s$	*B*	900 × 1	,,	915
$\delta_{2000} = +61^d02'20''$	*V*	600 × 1	,,	1190
	R	300 × 1	,,	1346
	I	300 × 1	,,	1585
Berkeley 11 – cluster	*U*	1800 × 2, 300 × 1	2000 November 18, 19	295
$\alpha_{2000} = 04^h20^m36^s$	*B*	1200 × 3, 240 × 1	,,	650
$\delta_{2000} = +44^d55'58''$	*V*	900 × 3, 180 × 1	,,	750
	R	600 × 3, 120 × 1	,,	930
	I	300 × 3, 60 × 1	,,	1090
Berkeley 11 – field	*U*	900 × 1	2000 November 20, 21	90
$\alpha_{2000} = 04^h20^m34^s$	*B*	600 × 1	,,	299
$\delta_{2000} = +44^d40'08''$	*V*	600 × 1	,,	474
	R	300 × 1	,,	676
	I	300 × 1	,,	723

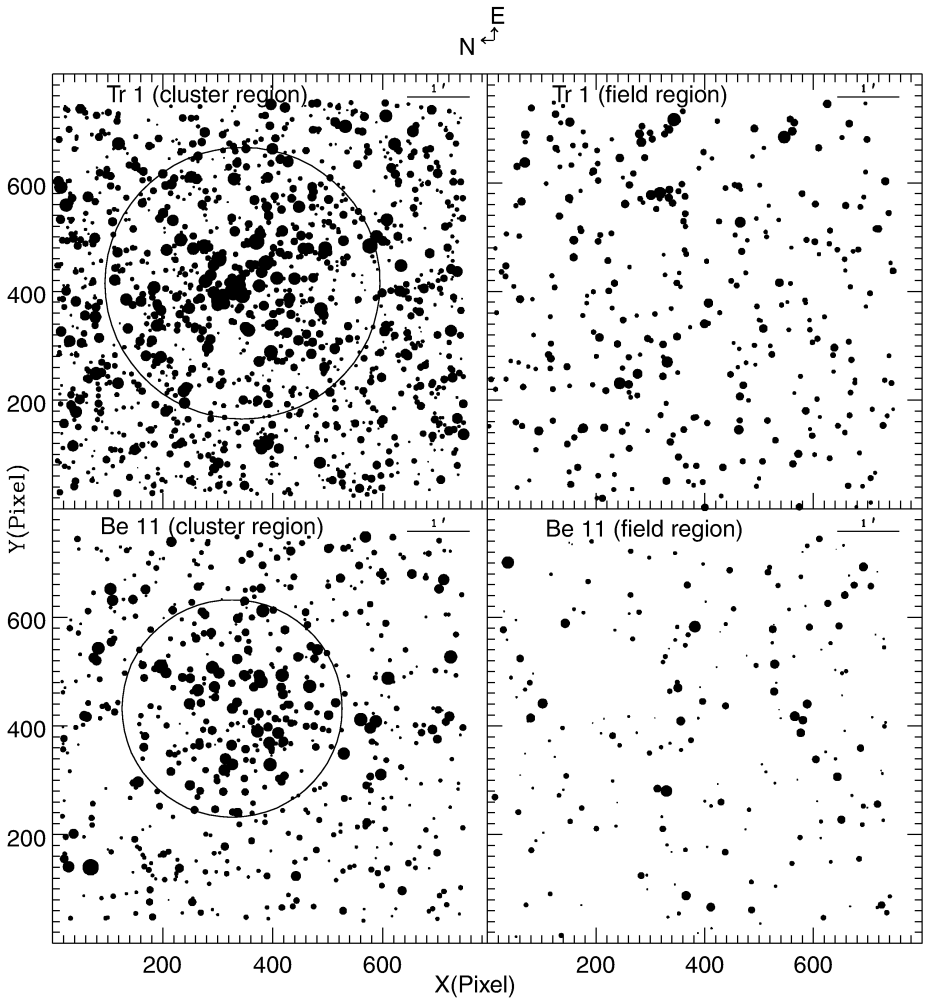

Figure 1. Identification maps for the cluster and field regions of Tr 1 and Be 11. The (X, Y) coordinates are in pixel units corresponding to 0.72 arcsec on the sky. East is up and north is left. Filled circles of different sizes represent the brightness of the stars. The smallest size denotes stars of $V \sim 21$ mag. Open circles in the clusters region represent the cluster size.

uncontaminated stars. In those cases where brighter stars are saturated on deep exposure frames, their magnitudes have been taken only from the short exposure frames. Wherever more than one measurement is available in a passband for a star, the final magnitude is an average of the individual measurements and its error is the ALLSTAR error of the average. When only one measurement was available, the error was taken to be the output of ALLSTAR.

The photometric calibration equations are determined by fitting a least-squares linear regression to the standard *UBVRI* photometric indices as a function of the observed instrumental magnitudes normalized for 1-s exposure time. The following colour equations are obtained for the system:

$$\Delta(U-B) = (0.973 \pm 0.020)\Delta(u-b)_0$$
$$\Delta(B-V) = (1.117 \pm 0.014)\Delta(b-v)_0$$
$$\Delta(V-R) = (0.886 \pm 0.011)\Delta(v-r)_0$$
$$\Delta(V-I) = (0.992 \pm 0.007)\Delta(v-i)_0$$
$$\Delta V = \Delta v_0 - (0.060 \pm 0.024)(V-I),$$

where Δ denotes differential values; $(U-B)$, $(B-V)$, $(V-R)$, $(V-I)$ and V are standard values taken from Landolt (1992) and $(u-b)_0$, $(b-v)_0$, $(v-r)_0(v-i)_0$ and v_0 are the instrumental CCD aperture magnitudes and colours corrected for atmospheric extinction. The atmospheric extinction coefficients are 0.59 ± 0.07, 0.37 ± 0.02, 0.29 ± 0.06, 0.16 ± 0.03 and 0.13 ± 0.02 for U, B, V, R and I, respectively. The errors in the colour coefficients are obtained from the deviation of data points from the linear relation. These equations are used to standardize the CCD instrumental magnitudes of both cluster and field regions. To establish the local standards, we selected several isolated stars in the observed regions and used the DAOGROW program for the construction of an aperture growth curve required for determining the difference between aperture and profile-fitting magnitudes. These differences and differences in exposure times and atmospheric extinctions are used in evaluating zero-points for the reference frames. The zero-points are uncertain by $\sim$0.02 mag in V; $\sim$0.01 mag in $(B-V)$, $(V-R)$, $(V-I)$ and $\sim$0.03 mag in $(U-B)$. Other factors contributing to the photometric uncertainty were described recently by Moitinho (2001). Amongst them, the internal errors estimated on theS/N ratio of the stars as output of ALLSTAR mainly produce the scatter in the various CC and CM diagrams of the clusters. They are given in Table 3 as a function of brightness for the cluster region. The errors become large

Table 3. Internal photometric errors as a function of brightness. σ is the standard deviation per observation in magnitude.

Magnitude range	σ_U	σ_B	σ_V	σ_R	σ_I
$\leqslant$12.0	0.012	0.001	0.005	0.003	0.011
12.0–13.0	0.013	0.004	0.008	0.008	0.013
13.0–14.0	0.019	0.006	0.010	0.009	0.019
14.0–15.0	0.021	0.007	0.014	0.012	0.014
15.0–16.0	0.023	0.012	0.015	0.013	0.014
16.0–17.0	0.025	0.012	0.017	0.015	0.020
17.0–18.0	0.043	0.024	0.026	0.025	0.030
18.0–19.0	0.083	0.054	0.055	0.051	0.060
19.0–20.0	0.086	0.095	0.102	0.091	0.113
20.0–21.0	0.158	0.281	0.356	0.346	0.264

($\geqslant$0.1 mag) for stars fainter than $V = 20$ mag, so the measurements should be considered unreliable below this magnitude.

The (X, Y) pixel coordinates as well as the V, $(U-B)$, $(B-V)$, $(V-R)$ and $(V-I)$ magnitudes of a sample of stars observed in the cluster and field regions of Tr 1 and Be 11 are listed in Tables 4 and 5, respectively. Only samples of the tables are presented here; the full tables are available in the electronic version of the article on *Synergy*, on the open star cluster data base web site at http://obswww.unige.ch/webda/, and also from the authors. In order to avoid introducing a new numbering system in Tr 1, we adopt the numbers from the data base given by Phelps & Janes (1994). Stars not observed earlier have a number starting with 1001 in Tr 1.

3.2 Comparison with the previous photometries

We compare the present data with the published CCD and photoelectric data. Table 6 represents the average differences in the sense 'present minus others' along with their standard deviations. The differences Δ in magnitude and colour are plotted in Fig. 2. Fig. 2 and Table 6 indicate that the present CCD data for Tr 1 show a constant zero-point offset of $\sim$0.08 mag in ΔV compared with that given by Phelps & Janes (1994). A weak linear dependence of $\Delta(B-V)$ is observed on brightness. The $\Delta(U-B)$ values, on the other hand, show a decreasing trend up to $V \sim 16.0$ mag but increase for fainter stars. As the *UBV* photoelectric data are in good agreement with the present CCD data for both the clusters, we suspect that there was calibration problem with the Phelps & Janes (1994) CCD data.

3.3 Near-IR data

The near-IR *JHK* data are taken from the digital Two Micron All-sky Survey (2MASS) available at the web site http://www.ipac.caltech.edu/2MASS/. 2MASS is uniformly scanning the entire sky in three near-IR bands J (1.25 μm), H (1.65 μm) and K_s (2.17 μm) with two highly automated 1.3-m telescopes equipped with a three-channel camera, each channel consisting of a 256 × 256 array of HgcdTe detectors. The photometric uncertainty of the data is <0.155 mag with $K_s \sim 16.5$ mag photometric completeness. The K_s magnitudes are converted into K magnitude following Persson et al. (1998). Further details concerning 2MASS and its data are available at http://www.ipac.caltech.edu/2mass/releases/second/doc/ explsup.html. The JHK_s data are available for 200 stars in the observed area of the Be 11 cluster. Among them only 179 stars are in common with our optical data.

4 DATA ANALYSIS

4.1 Cluster radius and radial stellar surface density

The first step in determining the cluster radius is to find its centre in the image. The centre of the cluster is determined iteratively by calculating average X and Y positions of the stars to within 300 pixels from an eye-estimated centre, until they converged to a constant value. An error of a few tens of pixels is expected in locating the cluster centre. The (X, Y) pixel coordinates of the cluster centres obtained in this way are (345, 415) and (326, 432) for Tr 1 and Be 11, respectively. The corresponding equatorial coordinates are given in Table 2. To determine the radial surface density of stars $\rho(r)$ in a cluster, the imaged area has been divided into a number of concentric circles with respect to the above estimated centre, in such a way that each zone contains a statistically significant number of stars. The number density of stars, ρ_i, in the ith zone has been calculated as $\rho_i = N_i/A_i$, where N_i is the number of stars and A_i is the area of the ith zone. The density versus radius plots for Tr 1 and

Table 4. CCD relative (X, Y) positions and V, $(U-B)$, $(B-V)$, $(V-R)$ and $(V-I)$ photometric magnitudes of a few stars, as a sample measured in the cluster and field region of the cluster Tr 1. In the cluster region, stars observed earlier have the numbering system of Phelps & Janes (1994) taken from the cluster data base, while the numbering of stars observed for the first time by us start with 1001 in column 1. The final column represents the photometric membership information where m and nm represent the member and non-member stars, respectively. In the field region, stars are numbered in increasing order of X value. The full version of this table is available in the electronic version of the article on *Synergy*.

Star	X (pixel)	Y (pixel)	V (mag)	$(U-B)$ (mag)	$(B-V)$ (mag)	$(V-R)$ (mag)	$(V-I)$ (mag)	Mem
				Tr 1 cluster region				
1001	97.64	229.68	19.80	*	1.21	0.72	1.49	nm
1002	356.27	238.04	18.67	0.42	1.16	0.66	1.35	m
1003	338.42	237.33	19.54	*	1.31	0.78	1.54	m
1004	309.76	235.40	18.04	0.48	1.17	0.66	1.31	m
1005	155.45	227.56	17.66	0.61	1.08	0.65	1.26	nm
				Tr 1 field region				
1	3.32	151.93	19.36	*	1.20	0.68	1.46	
2	6.93	238.09	18.45	*	1.23	0.67	1.45	
3	14.91	479.27	19.46	*	1.21	0.73	1.60	
4	15.22	219.91	18.94	*	1.37	0.67	1.52	
5	16.93	360.70	19.06	*	1.30	0.65	1.46	

Table 5. CCD relative (X, Y) positions and V, $(U-B)$, $(B-V)$, $(V-R)$ and $(V-I)$ photometric magnitudes of a few stars, as a sample measured in the cluster and field regions of the cluster Be 11. Stars are numbered in increasing order of X value. The final column indicates the photometric member and non-member stars of the cluster. The full version of this table is available in the electronic version of the article on *Synergy*.

Star	X (pixel)	Y (pixel)	V (mag)	$(U-B)$ (mag)	$(B-V)$ (mag)	$(V-R)$ (mag)	$(V-I)$ (mag)	Mem
			Be 11 cluster region					
142	311.95	318.82	14.78	0.61	0.99	0.48	1.04	m
143	312.78	178.07	16.97	0.77	1.30	0.63	1.33	m
144	313.98	339.75	15.11	0.43	0.91	0.45	0.97	m
145	316.18	128.17	18.53	*	1.54	0.77	1.65	nm
146	317.11	151.06	19.43	*	1.81	0.92	1.88	m
			Be 11 field region					
1	14.00	268.90	18.02	*	2.10	1.15	2.40	
2	29.36	577.23	17.64	0.60	1.10	0.62	1.29	
3	30.76	610.82	20.98	*	*	0.84	1.65	
4	36.19	558.98	20.62	*	*	0.77	1.56	
5	37.84	701.05	14.40	0.63	1.10	0.50	1.06	

Table 6. Comparison of our photometry with others for the clusters Tr 1 and Be 11. The difference (Δ) is always in the sense 'present minus comparison data'. The mean and standard deviations in magnitude are based on N stars. A few deviating points are not included in the average determination.

Cluster	Comparison data	V range	$\langle\Delta V\rangle$ mean $\pm\sigma$ (N)	$\langle\Delta(B-V)\rangle$ mean $\pm\sigma$ (N)	$\langle\Delta(U-B)\rangle$ mean $\pm\sigma$ (N)
Tr 1	Phelps & Janes (1994)	<14.0	$0.05 \pm 0.02(7)$	$0.03 \pm 0.01(6)$	$0.16 \pm 0.06(6)$
		14.0–15.0	$0.06 \pm 0.02(17)$	$0.04 \pm 0.02(17)$	$0.07 \pm 0.07(14)$
		15.0–16.0	$0.05 \pm 0.06(19)$	$0.02 \pm 0.02(16)$	$0.02 \pm 0.07(15)$
		16.0–16.5	$0.08 \pm 0.02(12)$	$0.01 \pm 0.03(12)$	$0.03 \pm 0.05(12)$
		16.5–17.0	$0.08 \pm 0.03(10)$	$0.03 \pm 0.03(10)$	$0.11 \pm 0.07(10)$
		17.0–17.5	$0.08 \pm 0.03(14)$	$0.01 \pm 0.08(13)$	$0.13 \pm 0.10(11)$
		17.5–18.0	$0.08 \pm 0.04(37)$	$-0.03 \pm 0.05(37)$	$0.12 \pm 0.09(29)$
		18.0–18.5	$0.08 \pm 0.05(30)$	$-0.03 \pm 0.09(30)$	$0.10 \pm 0.11(13)$
		18.5–19.0	$0.07 \pm 0.03(43)$	$-0.02 \pm 0.07(43)$	
	Joshi & Sagar (1977)	12.0–13.0	$-0.01 \pm 0.14(3)$	$0.03 \pm 0.04(4)$	$0.03 \pm 0.07(4)$
		13.0–14.0	$0.00 \pm 0.06(10)$	$0.05 \pm 0.04(12)$	$0.04 \pm 0.07(12)$
		14.0–15.0	$0.03 \pm 0.09(7)$	$0.07 \pm 0.08(17)$	$0.03 \pm 0.08(17)$
Be 11	Jackson et al. (1980)	13.0–14.0	$-0.05 \pm 0.02(6)$	$0.00 \pm 0.01(6)$	$-0.03 \pm 0.01(6)$
		14.0–15.0	$-0.03 \pm 0.01(7)$	$-0.03 \pm 0.01(7)$	$-0.02 \pm 0.03(7)$
		15.0–16.0	$-0.03 \pm 0.02(5)$	$-0.02 \pm 0.03(5)$	$-0.02 \pm 0.04(5)$

Be 11 are shown in Fig. 3. A clear radius–density gradient present in Fig. 3 confirms the existence of clustering. Following Kaluzny (1992), we describe the $\rho(r)$ of an open cluster as

$$\rho(r) \propto \frac{f_0}{1+(r/r_c)^2},$$

where the cluster core radius r_c is the radial distance at which the value of $\rho(r)$ becomes half of the central density f_0. We fit this function to the observed data points of each cluster and use a χ^2-minimization technique to determine r_c and other constants. As can be seen in Fig. 3, the fitting of the function is satisfactory. The values of core radii derived in this way are 85 ± 10 and 180 ± 10 pixels for Tr 1 and Be 11, respectively. Fig. 3 also separates the cluster region from the surrounding field region. The field star densities thus obtained are 2.2×10^{-3} and 1.0×10^{-3} star pixel^{-2} for Tr 1 and Be 11, respectively. The radial distribution of stars in Tr 1 and Be 11 indicates that the extent of the cluster is about 250 and 200 pixels, respectively, which correspond to ~3.0 and 2.4 in arcmin. The cluster sizes are thus a few times larger than the corresponding core sizes, which is in agreement with the findings of Nilakshi et al. (2002).

4.2 Apparent colour–magnitude diagrams of cluster and field regions

The apparent CM diagrams generated from the present data for the Tr 1 and Be 11 clusters and their field regions are displayed in Fig. 4. The CM diagrams extend up to $V \sim 21$ mag except in the V, $(U-B)$ diagram where it is only up to $V \sim 18$ mag. A well-defined cluster main sequence (MS) contaminated by field stars is clearly visible in all CM diagrams. The field star contamination increases with decreasing brightness. The cluster sequence fainter than $V \sim 17$ mag has a larger scatter. This may be caused by photometric errors as well as field star contamination. It is difficult to separate field stars from the cluster members only on the basis of their closeness to the main populated area of the CM diagrams, because field stars at cluster distance and reddening also occupy this area (see Fig. 4). For the separation of cluster members from the field stars, precise proper motion and/or radial velocity measurements of these stars are required. In the absence of such data, we use a photometric criterion to separate obvious field stars. A star is considered as a non-member if it lies outside the cluster sequence in at least one CC or CM diagram. From the V, $(V-I)$ diagram of the field region, number

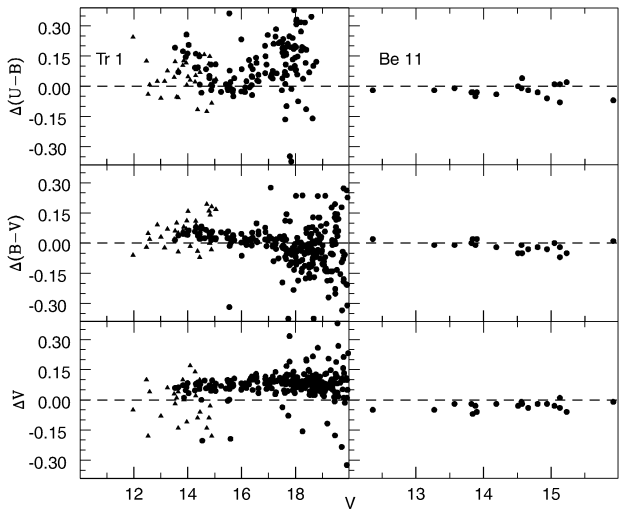

Figure 2. A comparison of the present photometry with CCD and photoelectric data of Tr 1 and Be 11. For Tr 1, filled circles represent the CCD data of Phelps & Janes (1994) and triangles represent the photoelectric data of Joshi & Sagar (1977). For Be 11 filled circles represent the photoelectric data of Jackson et al. (1980).

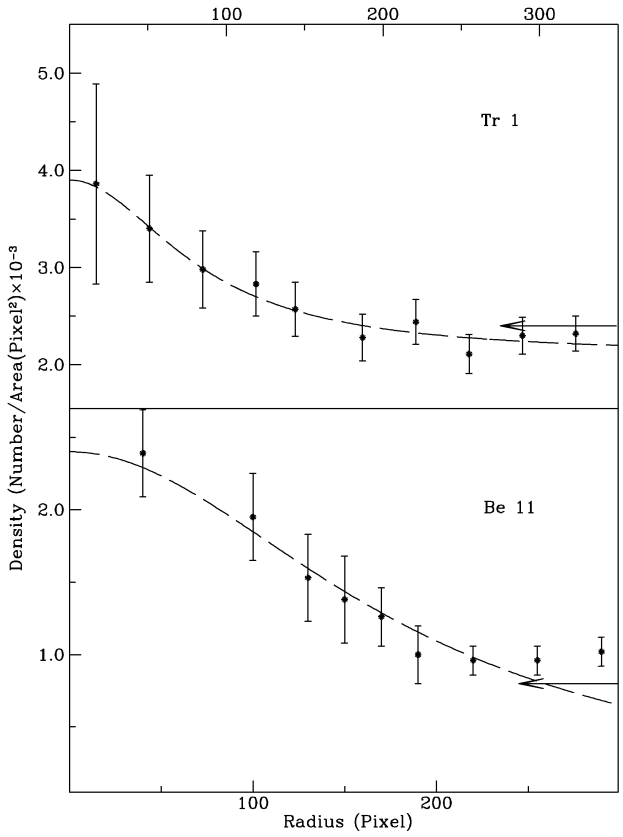

Figure 3. The radial density profile for Tr 1 and Be 11. The length of the error bar denotes errors resulting from sampling statistics ($=1/\sqrt{N}$, where N is the number of stars used in the density estimation at that point). Dotted curves represent the fitted profile and arrows represent the level of field star densities.

of field stars expected statistically among the photometric cluster members has been given in Table 7. The frequency distribution of the field star contamination in different parts of the CM diagram can be estimated from Table 7. It is thus clear that all photometric probable members cannot be cluster members and non-members should be subtracted in the studies of cluster MF, etc. However, probable members located within a cluster radius from its centre can be used to determine the cluster parameters, as they have relatively less field star contamination and this has been done in the sections to follow.

4.3 Interstellar extinction in the direction of clusters

To estimate interstellar extinction in the direction of the clusters, we plot in Fig. 5 $(U-B)$ versus $(B-V)$ diagrams of the sample stars. Adopting the slope of the reddening line $E(U-B)/E(B-V)$ as 0.72, we fit the intrinsic zero-age main sequence (ZAMS) given by Schmidt-Kaler (1982) to the MS stars of spectral type earlier than A0. This gives a mean value of $E(B-V)=0.60\pm0.05$ mag for the cluster Tr 1 and 0.95 ± 0.05 mag for the cluster Be 11. Our reddening estimates for the imaged region agree fairly well with the values estimated earlier by others (see Table 1).

To determine the nature of the interstellar extinction law in the direction of clusters, we used the stars with spectral type earlier than A0. This has been selected from their location in the $(U-B)$ versus $(B-V)$ and apparent CM diagrams, which reveals that bright stars ($V<15.0$ mag) with $(B-V)<0.90$ mag in Tr 1 and with $(B-V)<1.30$ mag in Be 11 are the required objects. For these stars, their intrinsic colours have been determined using either the spectral type (available only for 15 stars in Be 11) taken from the open cluster data base (cf. Mermilliod 1995) or the *UBV* photometric *Q*-method (cf. Johnson & Morgan 1953; Sagar & Joshi 1979) and the calibrations given by Caldwell et al. (1993) for $(U-B)_0$, $(V-R)_0$ and $(V-I)_0$ with $(B-V)_0$. The mean values of the colour excess ratios derived in this way are listed in Table 8 for both the clusters. They indicate that the law of interstellar extinction in the direction of the clusters under discussion is normal.

4.3.1 *Presence of non-uniformity in* $E(B-V)$

In order to see the extent of non-uniform extinction in the clusters under study, we plot histograms of $E(B-V)$ in Fig. 6. They indicate that there is a range of ~0.4 mag in $E(B-V)$ values of both the cluster stars with a peak around $E(B-V)=0.65$ and 0.95 mag for Tr 1 and Be 11, respectively.

To determine the presence of non-uniform extinction in a cluster, we calculate the value of $\Delta E(B-V)=E(B-V)_{\rm max}-E(B-V)_{\rm min}$, where $E(B-V)_{\rm max}$ and $E(B-V)_{\rm min}$ are determined on the basis of the five highes and five lowest $E(B-V)$ values of the MS cluster members, respectively. In this way we can find the values of $\Delta E(B-V)$ and these values are listed in Table 9. As the factors other than non-uniform extinction such as stellar evolution, stellar duplicity, stellar rotation, difference in chemical composition, dispersion in ages, distances and uncertainty in photometric data (cf. Burki 1975; Sagar 1987; Yadav & Sagar 2001) can produce a maximum dispersion in $E(B-V)$ of ~0.11 mag for MS members, we consider the presence of non-uniform extinction in both cluster regions, as the observed values of $\Delta E(B-V)$ for their MS stars are much greater than 0.11 mag. In order to see whether it is a result of the presence of varying amounts of matter inside them or a result of any other regions, we studied below the variation of $E(B-V)$ with spatial position of stars in the clusters.

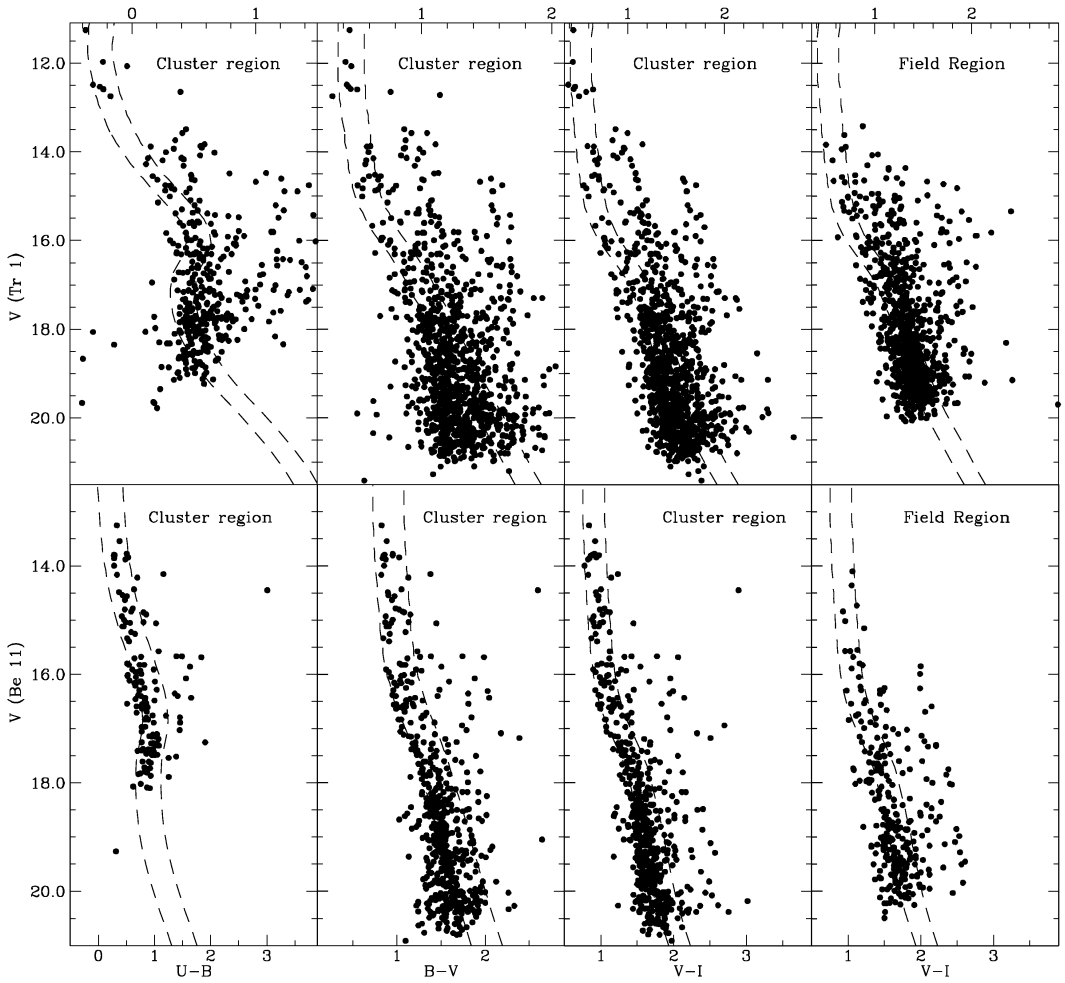

Figure 4. The V, $(U-B)$, V, $(B-V)$ and V, $(V-I)$ diagrams for the stars observed by us in Tr 1 and Be 11 cluster regions and the V, $(V-I)$ CM diagram of the corresponding field regions. Dotted lines represent the blue and red envelope of the cluster MS.

Table 7. Frequency distribution of the stars in the V, $(V-I)$ diagram of the cluster and field regions. N_B, N_S and N_R denote the number of stars in a magnitude bin blueward, along and redward of the cluster sequence, respectively. N_C (difference between the N_S value of cluster and field regions) denotes the statistically expected number of cluster members in the magnitude bin.

V range	Tr 1							Be 11						
	Cluster region			Field region				Cluster region			Field region			
	N_B	N_S	N_R	N_B	N_S	N_R	N_C	N_B	N_S	N_R	N_B	N_S	N_R	N_C
13–14	0	8	8	1	3	1	5	0	10	0	0	0	0	10
14–15	0	20	25	0	3	21	17	0	16	4	0	4	0	12
15–16	0	22	40	1	5	60	17	0	26	10	0	8	1	18
16–17	3	37	53	4	25	80	12	0	48	14	6	9	10	39
17–18	18	97	75	24	74	74	23	0	68	15	22	16	14	52
18–19	52	131	71	80	110	52	21	14	142	19	33	22	14	120
19–20	130	139	51	105	110	28	29	45	159	14	68	34	14	125

4.3.2 *Spatial variation of $E(B-V)$*

To study the spatial variation of reddening in terms of $E(B-V)$ across the cluster region, we divide the cluster field into small boxes of size 1.0×1.0 arcmin^2. The positional variation of $E(B-V)$ is shown in Table 10 for both clusters. An inspection of Table 10 indicates that $E(B-V)$ does not show any systematic variation with position in both clusters. However, it varies randomly, which may be a result of the random distribution of gas and dust within the clusters.

4.3.3 *Interstellar extinction in the near-IR*

In order to derive the interstellar extinction for Be 11 in near-IR region, we have combined optical and infrared data. There are 47

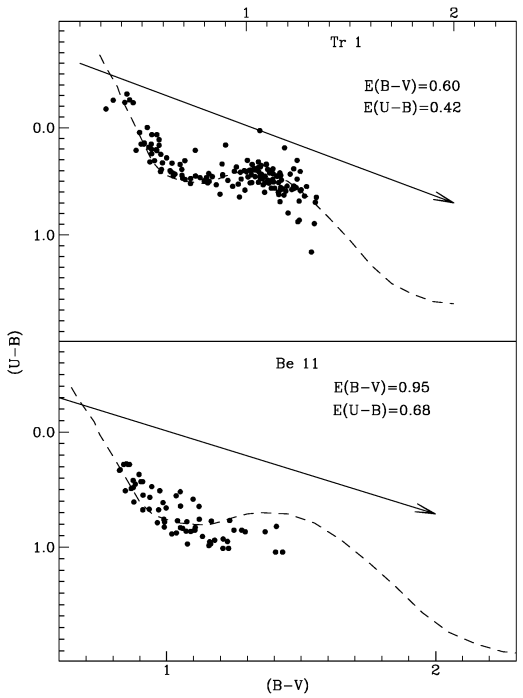

Figure 5. The $(U-B)$ versus $(B-V)$ diagrams of the stars in cluster region observed by us for Tr 1 and Be 11. The continuous straight line represents slope 0.72 and direction of the reddening vector. The dotted curve represents the locus of Schmidt–Kaler's (1982) ZAMS fitted for the marked values of colour excess.

Table 8. A comparison of the colour excess ratios with $E(B-V)$ for star clusters with the corresponding values for the normal interstellar extinction law given by Cardelli et al. (1989).

Objects	$\frac{E(U-B)}{E(B-V)}$	$\frac{E(V-R)}{E(B-V)}$	$\frac{E(V-I)}{E(B-V)}$
Normal interstellar	0.72	0.60	1.25
Tr 1	0.72 ± 0.03	0.54 ± 0.02	1.13 ± 0.05
Be 11	0.71 ± 0.02	0.45 ± 0.02	1.04 ± 0.04

common stars within the cluster radius. We construct in Fig. 7 a $(J-K)$ versus $(V-K)$ diagram for the stars within the cluster radius and fit a ZAMS for metallicity $Z=0.02$ taken from Schaller et al. (1992). This yields $E(J-K)=0.40\pm0.20$ mag and $E(V-K)=2.20\pm0.20$ mag, which corresponds to a ratio $\frac{E(J-K)}{E(V-K)}=0.18\pm0.30$, in good agreement with the normal interstellar extinction value 0.19 suggested by Cardelli, Clayton & Mathis (1989). However, scattering is larger owing to the error size in *JHK* data.

4.3.4 *Extinction Law in Be 11*

In order to see the nature of the extinction law in Be 11, we plot the colour excess $E(U-B)$, $E(B-V)$, $E(V-R)$, $E(V-I)$, $E(V-H)$ and $E(V-K)$ against $E(V-J)$ in Fig. 8. For normalization we have used the colour excess $E(V-J)$ instead of $E(B-V)$, because $E(V-J)$ does not depend on properties such as the chemical composition, shape, and structure and degree of alignment of the interstellar matter (Sagar & Qian 1990). Also, they are a better measure of the total amount of interstellar extinction because of their larger values compared with either near-IR or optical

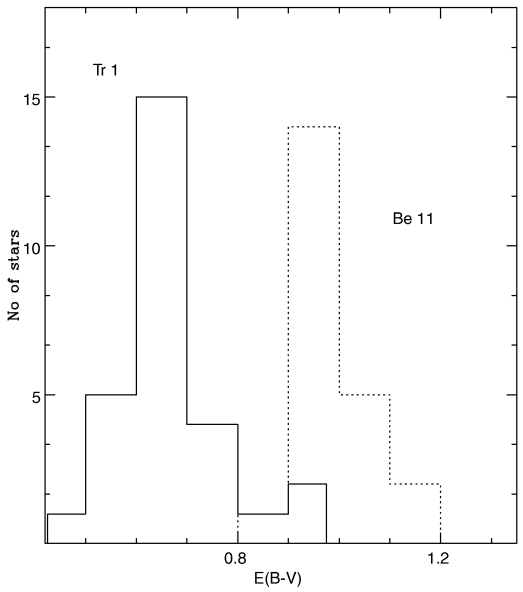

Figure 6. The solid and dotted lines represent the histograms of $E(B-V)$ for Tr 1 and Be 11, respectively. They indicate the presence of non-uniform extinction in both clusters.

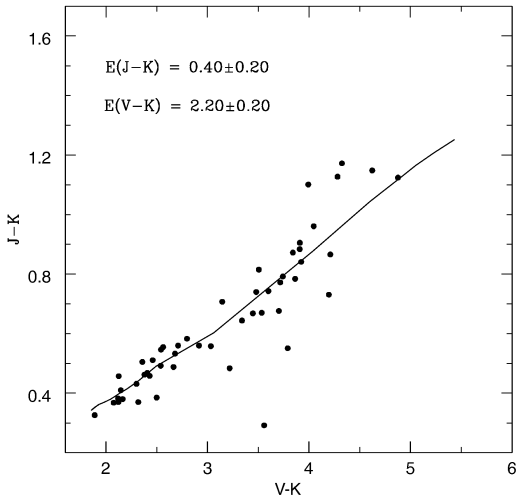

Figure 7. The $(J-K)$ versus $(V-K)$ colour–colour diagram of all the stars which are common in *V* and *JHK* data within the cluster radius for the cluster Be 11. The solid line is a ZAMS fitted for the marked values of colour excess.

Table 9. The values of $E(B-V)_{\rm min}$, $(B-V)_{\rm max}$ and $\Delta E(B-V)$ (see text).

Cluster	$E(B-V)_{\rm min}$ (mag)	$E(B-V)_{\rm max}$ (mag)	$\Delta E(B-V)$ (mag)
Tr 1	0.55	0.85	0.30
Be 11	0.91	1.06	0.15

colour excesses. A careful selection is needed in the case of colour excesses, because the young clusters are embedded in emission nebulosity and also contains young stellar objects. In such an environment, the blueing effect, ultraviolet excess, circumstellar dust and

Table 10. Spatial variation of $E(B-V)$ across the clusters Tr 1 and Be 11. The mean values of $E(B-V)$ with their standard deviation in magnitude in $\times 1$ arcmin^2 areas are indicated in the appropriate boxes, with the number of stars used for this purpose given in parentheses. The $\Delta\alpha$ and $\Delta\delta$ values are in arcmin relative to the cluster centre given in Table 2.

$\Delta\alpha \rightarrow$ / $\Delta\delta \downarrow$	−3 to −2	−2 to −1	−1 to 0	0 to 1	1 to 2
			Tr 1		
−3 to −2	–	0.60 (1)	–	–	–
−2 to −1	–	0.60 (1)	–	0.73 ± 0.21 (3)	–
−1 to 0	0.66 (1)	0.61 (1)	0.60 ± 0.09 (5)	0.58 (1)	0.53 (1)
0 to 1	–	0.67 ± 0.07 (2)	0.65 ± 0.04 (3)	0.85 ± 0.20 (2)	0.67 ± 0.07 (3)
1 to 2	–	0.68 (1)	– –	– –	0.64 (1)
2 to 3	–	0.79 (1)	0.71 (1)	–	–
			Be 11		
−2 to −1	–	–	1.01 ± 0.02 (2)	1.00 ± 0.01 (2)	–
−1 to 0	–	–	0.95 (1)	0.95 ± 0.05 (2)	1.03 (1)
0 to 1	–	1.05 ± 0.20 (2)	0.98 ± 0.04 (5)	0.94 ± 0.05 (3)	0.99 ± 0.01 (2)
1 to 2	–	–	–	–	–
2 to 3	–			0.94 (1)	–

gas shells, etc., may be present in and around the cluster stars. So, it is fruitful to use V band rather than the U or B bands, because it is least affected in such cases. Similarly, in the near-IR, the J band is preferred, with a view to minimizing the contributions from the possible presence of circumstellar material, etc., around young stellar objects and also to choose a photometric band that most closely represents the emission from the stellar photosphere. We have therefore estimated the colour excess ratios relative to $E(V-J)$.

In Fig. 8, solid line represents the least-squares linear fits to the data points. The values of correlation coefficient (r) and fit indicate that the data points are well represented by a linear relation. The slopes of these straight lines represent reddening directions in the form of colour excess ratios are given in Table 11. For comparison, the colour excess ratios given by Cardelli et al. (1989) are also listed in Table 11. The present reddening directions agree well with those given for a normal interstellar extinction law.

In Fig. 9, we have plotted ratios $E(V-K)/E(B-V)$ and $E(V-K)/E(V-J)$ against $E(V-K)$. The horizontal line in the figure represents the value of the ratio for the normal interstellar extinction law. In the case of a normal extinction law, the ratio $E(V-K)/E(B-V)$ and $E(V-K)/E(V-J)$ remains the same for all the values of $E(V-K)$ (Sagar & Qian 1990). Least-squares linear fits to the data points give:

$$E(V-K)/E(B-V) = 0.10(\pm 0.03)E(V-K) + 2.13(\pm 0.31)$$

$$r = 0.29$$

$$E(V-K)/E(V-J) = 0.03(\pm 0.02)E(V-K) + 1.18(\pm 0.05)$$

$$r = 0.44.$$

The values of r are <0.5. This indicates that the relations are not statistically significant. This may therefore imply the absence of an anomalous interstellar extinction law toward the cluster Be 11.

In the absence of complete data at long wavelengths, the approximation $R = 1.1E(V-K)/E(B-V)$ suggested by Whittet & Breda (1980) is generally used to deduce R. It is relatively insensitive to the reddening law adopted. We have therefore used this relation to evaluate R. The average value of $R = 2.60 \pm 0.34$ (sd), which is not too different from the value of 3.1 for a normal extinction law. In light of the above analysis, we conclude that the interstellar extinction law is normal towards Be 11 in agreement with our earlier result.

4.4 Distance to the clusters

The distances of the clusters are derived by a ZAMS fitting procedure. We have plotted intrinsic CM diagrams for Tr 1 and Be 11 in Fig. 10. In order to reduce field star contamination, we have used only those probable cluster member stars that are within the cluster radius from the cluster centre. For plotting these diagrams, we have converted the apparent V magnitude and $(U-B)$, $(B-V)$, $(V-R)$ and $(V-I)$ colours into the intrinsic magnitude using the available individual values of $E(B-V)$ and following the relations for $E(U-B)$ (cf. Kamp 1974; Sagar & Joshi 1979), A_v and $E(V-I)$ (Walker 1987) and $E(V-R)$ (Alcalá & Ferro 1988):

$$E(U-B) = [X + 0.05E(B-V)]E(B-V)$$

where

$$X = 0.62 - 0.3(B-V)_0 \quad \text{for} \quad (B-V)_0 < -0.09$$

and

$$X = 0.66 + 0.08(B-V)_0 \quad \text{for} \quad (B-V)_0 > -0.09.$$

Table 11. A comparison of the extinction law in the direction of Be 11 with the normal extinction law given by Cardelli et al. (1989).

Source	$\frac{E(U-B)}{E(V-J)}$	$\frac{E(B-V)}{E(V-J)}$	$\frac{E(V-R)}{E(V-J)}$	$\frac{E(V-I)}{E(V-J)}$	$\frac{E(V-H)}{E(V-J)}$	$\frac{E(V-K)}{E(V-J)}$	$\frac{E(J-K)}{E(V-K)}$
Cardelli et al.	0.32	0.43	0.27	0.56	1.13	1.21	0.19
Colour excess ratio	0.42 ± 0.13	0.53 ± 0.03	0.29 ± 0.03	0.56 ± 0.04	1.31 ± 0.07	1.38 ± 0.07	0.18 ± 0.30

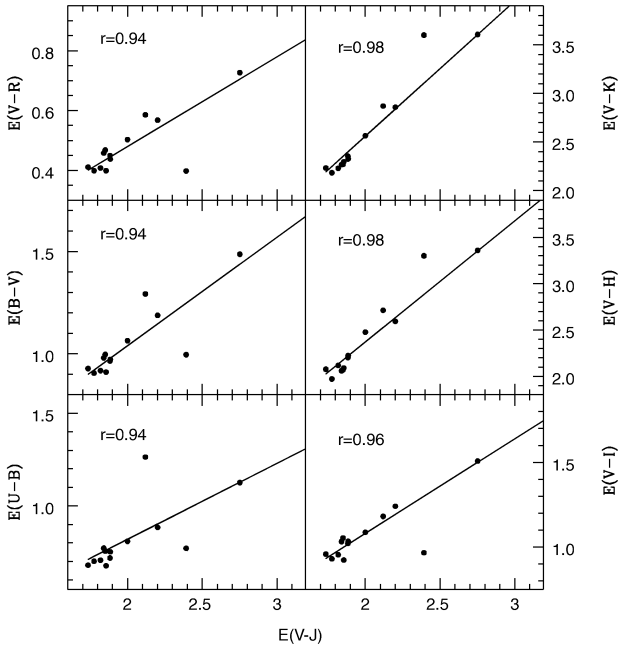

Figure 8. The plot of $E(U-B)$, $E(B-V)$, $E(V-R)E(V-I)$, $E(V-H)$ and $(V-K)$ against $E(V-J)$ for Be 11. The solid line in each diagram represents a least-squares linear fit to the data points. The values of correlation coefficients are shown in the diagram.

$$A_v = [3.06 + 0.25(B-V)_0 + 0.05E(B-V)]E(B-V);$$

and

$$E(V-R) = [\mathrm{E1} + \mathrm{E2}E(B-V)]E(B-V)$$

where

$$\mathrm{E1} = 0.6316 + 0.0713(B-V)_0$$

and

$$\mathrm{E2} = 0.0362 + 0.0078(B-V)_0;$$

$$E(V-I) = 1.25[1 + 0.06(B-V)_0 + 0.014E(B-V)]E(B-V).$$

For fainter stars, the average $E(B-V)$ value have been used for both the clusters since individual values are not known.

In the V_0, $(U-B)_0$ and V_0, $(B-V)_0$ diagrams, we fitted the ZAMS given by Schmidt-Kaler (1982), while the ZAMS given by Walker (1985) was fitted in the V_0, $(V-I)_0$ diagram. For the V_0, $(V-R)_0$ diagram, we have calculated $(V-R)_0$ using its relation with $(B-V)_0$ given by Caldwell et al. (1993). The visual fit of the ZAMS to the bluest envelope of the CM diagrams gives the mean values of $(m-M)_0$ as 12.1 ± 0.2 and 11.7 ± 0.2 mag for Tr 1 and Be 11, respectively. The distances to the clusters should be considered reliable because they have been derived by fitting the ZAMS over a wide range of the cluster MS. The distance modulus

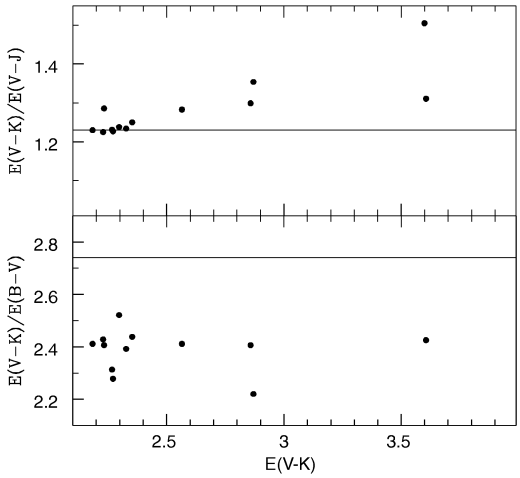

Figure 9. The colour excess ratios $E(V-K)/E(V-J)$ (top panel) and $E(V-K)/E(B-V)$ (bottom panel) as a function of $E(V-K)$ for Be 11. The horizontal lines are drawn for the normal values of the colour excess ratios.

determined above yields a distance of 2.6 ± 0.10 kpc to Tr 1 and of 2.2 ± 0.10 kpc to Be 11. For Tr 1, our values of distance modulus are in good agreement with the value of 12.10 given by Phelps & Janes (1994). However, it is slightly higher than the value of 11.64 mag given by Joshi & Sagar (1977). The present determination of the distance modulus to the cluster Be 11 agrees very well with the value of 11.7 mag given by Jackson et al. (1980).

4.5 Gaps in MS

The intrinsic CM diagrams of both the clusters Tr 1 and Be 11 exhibit gaps at different points in the MS (see Fig. 10). There seems to be a gap between 10.7 and 11.6 intrinsic V magnitude in Tr 1. Another feature seen in this cluster MS is the deficiency of stars between 14.0 and 14.8 mag. In the case of Be 11, we noticed a gap between 12.4 and 12.9 intrinsic V magnitude. The reality of the gaps in MS is tested by the method adopted by Hawarden (1971). The probability of finding such gaps accidentally is 0.3 per cent for the gap between 10.7 and 11.6 in Tr 1 and 0.02 per cent for the gap between 12.4 and 12.9 in Be 11. The accidental probability is 12 per cent for the fainter gap in Tr 1. The very low values of probabilities indicate that the observed gaps are real. However, the cause of such gaps are not well understood.

4.6 Ages of the clusters

The ages of the clusters Tr 1 and Be 11 have been determined by fitting the theoretical stellar evolutionary isochrones given by Schaller et al. (1992) in the corresponding CM diagrams (Fig. 10). The isochrones are for Population I stars ($X = 0.70$, $Y = 0.28$, $Z = 0.02$) and include the effects of mass loss and convective core overshooting in the model. The isochrone fitting to the main-sequence and

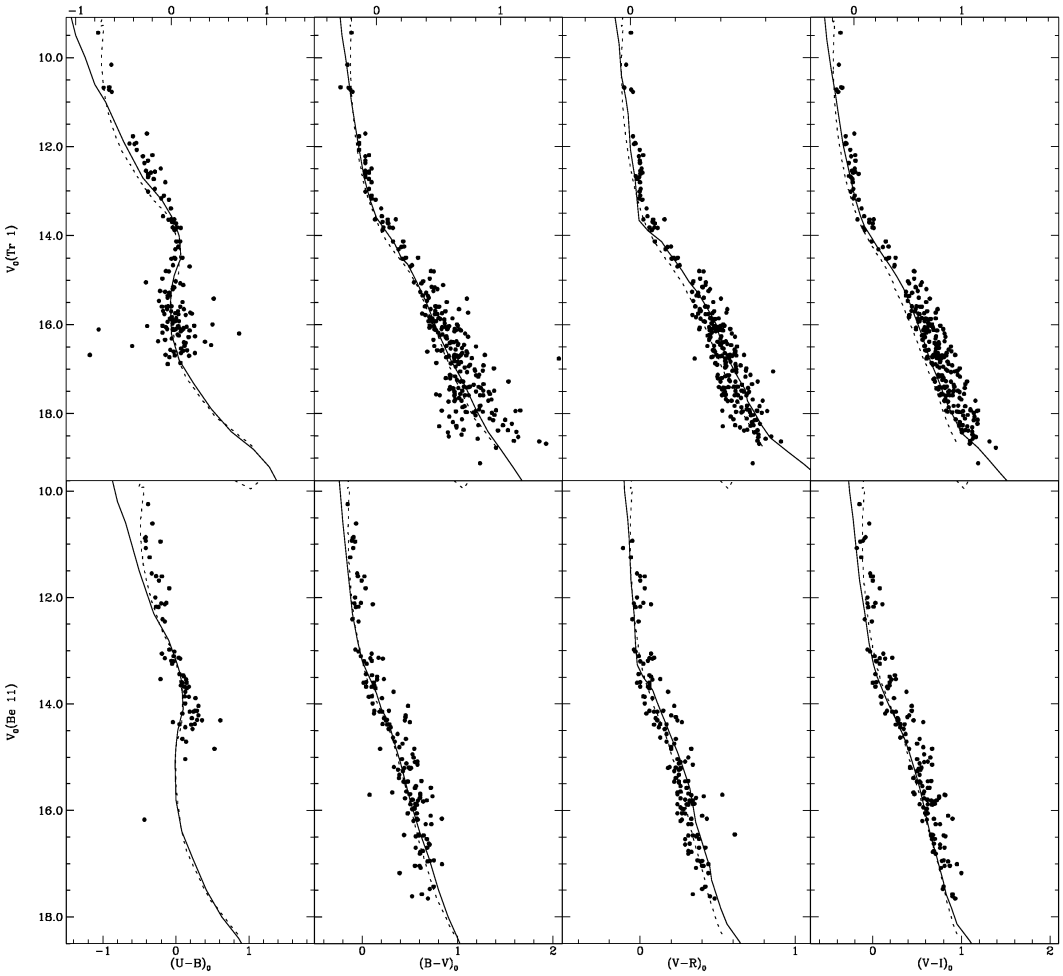

Figure 10. The V_0, $(U-B)_0$, V_0, $(B-V)_0$, V_0, $(V-R)_0$ and V_0, $(V-I)_0$ diagrams for stars of Tr 1 and Be 11. The continuous curves are the ZAMS fitted to the MS. The dotted curves are the isochrones for Population I stars of log(age) = 7.6 for Tr 1 and 8.05 for Be 11 fitted to the brighter cluster members.

brighter stars indicates that the ages of the clusters Tr 1 and Be 11 are 40 ± 10 and 110 ± 10 Myr, respectively. The present age estimates for Tr 1 and Be 11 are in good agreement with the values given in Mermilliod (1995) (see Table 1). For Tr 1, Joshi & Sagar (1977) have given the age 3×10^7 yr, which is also in good agreement.

To determine the age and distance of the cluster Be 11 with the combination of optical and near-IR data, we plot V versus $(V-K)$ and K versus $(J-K)$ in Fig. 11. We have overplotted the theoretical isochrones of log(age) = 8.05 given by Schaller et al. (1992). The apparent distance moduli $(m-M)_{V,(V-K)}$ and $(m-M)_{K,(J-K)}$ turn out to be 14.6 ± 0.3 and 12.0 ± 0.3 mag, respectively. By using the reddening estimated in the previous section we derive a distance of 2.1 ± 0.3 kpc for Be 11. Both age and distance determination for Be 11 are thus in excellent agreement with our earlier estimates.

4.7 Luminosity and mass function of the clusters

The luminosity function, denotes the relative number of stars in the unit magnitude range. The correction of non-member stars is very much important in the construction of LFs for star clusters. Two colours, such as B and V or V and I, are required for the non-member identification. We therefore need to construct the LF either from a V, $(B-V)$ diagram or from a V, $(V-I)$ diagram or from a similar diagram instead of from a single B, V or I or any other passband. We used the V, $(V-I)$ diagram rather than the others as it is deepest. The main disadvantage of using two passbands for the construction of the LF is that both passbands introduce incompleteness, for which the determination is a difficult process, as described below.

4.7.1 *Determination of photometric completeness*

The method consists of insertion of randomly selected artificial stars with known magnitude and position in the original V frame. For the I-band image the inserted stars have the same geometrical positions but differ in I brightness according to mean $(V-I)$ colour of the MS stars. Only 15 per cent of the actually detected stars are inserted at one time, so that the crowding characteristics of the original data remains almost unchanged. The luminosity distribution of the artificial stars has been chosen in such a way that more stars are inserted into the fainter magnitude bins. The frames are reprocessed using the same procedure used for the original frames. The ratio of recovered to inserted stars in the different magnitude bins gives the completeness factor (CF) for that region directly. Table 12 lists the CF in both cluster and field regions of the objects under study.

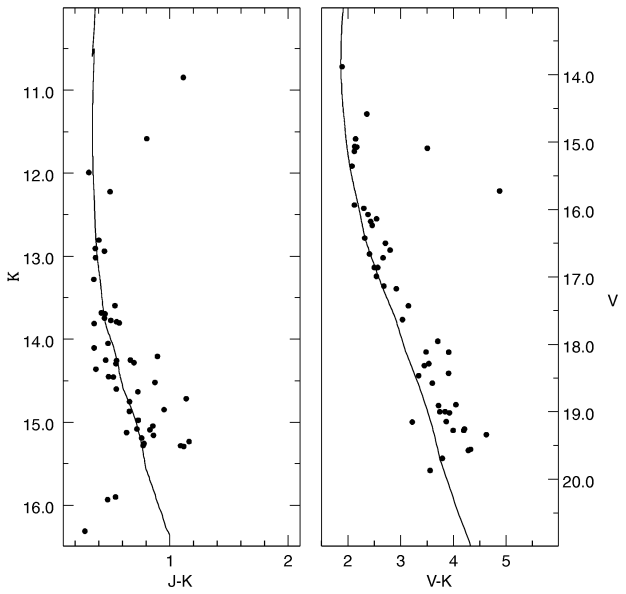

Figure 11. The K, $(J-K)$ and V, $(V-K)$ diagrams of the sample stars in cluster Be 11.

Table 12. Variation of completeness factor with the MS brightness in both cluster and field regions.

V mag range	Tr 1		Be 11	
	Cluster	Field	Cluster	Field
13–14	0.96	0.99	0.99	0.99
14–15	0.96	0.99	0.99	0.99
15–16	0.95	0.99	0.99	0.99
16–17	0.94	0.98	0.98	0.99
17–18	0.94	0.98	0.97	0.99
18–19	0.90	0.98	0.96	0.98
19–20	0.80	0.98	0.93	0.98

Several authors have discussed the method for determining the CF (cf. Stetson 1987; Mateo 1988; Sagar & Richtler 1991; Banks, Dodd & Sullivan 1995). Sagar & Richtler (1991) have taken the minimum value of the completeness factors of the pair to correct the star counts. They argue that the two frames are not independent and that the multiplicative assumption of Mateo (1988) could not be justified. Banks et al. (1995) tested the ability of the techniques given by Mateo (1988) and Sagar & Richtler (1991) on the basis of numerical simulations. They conclude that the product method of Mateo (1988) increasingly overestimates the incompleteness correction as the magnitude is increased, and the method suggested by Sagar & Richtler (1991) recovered the actual LF better with a mean error of 3 per cent up to CF > 0.5. We therefore used the procedure of Sagar & Richtler (1991) in the present work.

4.7.2 *Determination of mass function*

To derive the true LF of the cluster we have to remove the field star contamination. For this, we use a photometric criterion. First, we defined a blue and red envelope for the MS on the V, $(V-I)$ CM diagram. The same envelope was drawn on the corresponding field region. Star counts as a function of luminosity were made in both (cluster and field) regions. In this way we can estimate the number of field stars present in various magnitude bins of the cluster region. The observed LFs of the cluster and field regions were also corrected for data incompleteness as well as for differences in area. The true LF for the cluster was obtained by subtracting the observed LF of the field region from the observed LF of the cluster region.

The mass function (MF) denotes the relative number of stars in a unit range of mass centred on mass M. The MF slope has been derived from the mass distribution $\xi(M)$. If dN represents the number of stars in a mass bin dM with central mass M, then the value of slope x is determined from the linear relation

$$\log \frac{\mathrm{d}N}{\mathrm{d}M} = -(1+x) \times \log(M) + \text{constant}$$

using the least-squares solution. The Salpeter (1955) value for the slope of MF is $x = 1.35$.

To derive the MF from LF, we need theoretical evolutionary tracks and accurate knowledge of the cluster parameters such as reddening, distance, age, etc. Theoretical models from Schaller et al. (1992) were used to convert the observed LF to the MF. Fig. 12 represents the plot of MFs of Tr 1 and Be 11. The value of the MF slope along with the mass range and error are given in Table 13, where the quoted errors are errors resulting from the linear least-squares fit to the data points. For the cluster Tr 1, the value of x is in agreement with the value given by Phelps & Janes (1993). The values of x for both clusters are in agreement with the Salpeter value.

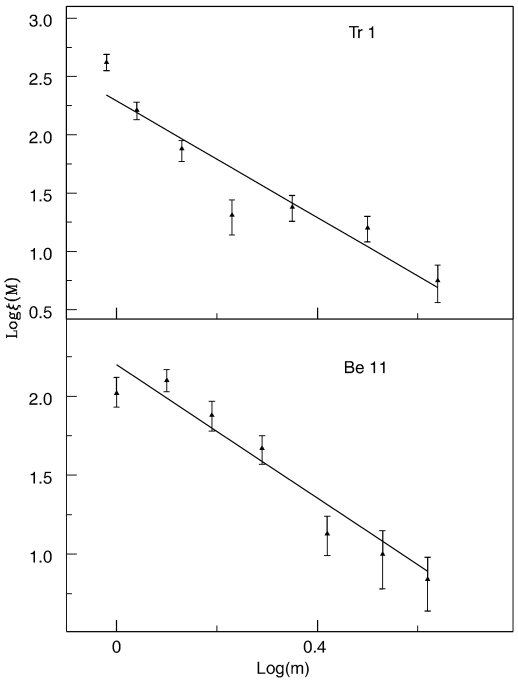

Figure 12. The plot shows the mass functions derived using the isochrones of Schaller et al. (1992).

Table 13. The slope of the mass function derived from LF along with relaxation time T_E.

Cluster	Mass range ($M_\odot$)	Mass function slope (x)	log T_E
Tr 1	0.9–5.1	1.50 ± 0.40	7.2
Be 11	1.0–4.5	1.22 ± 0.24	7.1

The dip is seen in the MF of both clusters. In the cluster Tr 1 one dip is present in the mass range $1.5 < M/M_{\odot} < 1.9$. This dip is caused by the deficiency of stars in the intrinsic V magnitude between 14.0 and 14.8 (see Section 4.5). In this cluster an apparent dip in LF is also found by Phelps & Janes (1993) at 1.4 $M_{\odot}$. One dip is also seen in the MF of Be 11 in the mass range $2.0 < M/M_{\odot} < 3.0$. This dip corresponds to the gap noticed in the intrinsic V magnitude between 12.4 and 12.9 (see Section 4.5).

5 MASS SEGREGATION

To study the effect of mass segregation for the clusters under study, we plot in Fig. 13 the cumulative radial stellar distribution of stars for different masses. A careful inspection of Fig. 13 shows that both clusters have a mass segregation effect.

To perform the Kolmogorov–Smirnov (K-S) test among these distribution to see whether or not they belong to the same distribution, we have divided the data into three mass ranges $5.0 \leqslant M_{\odot} < 2.5$, $2.5 \leqslant M_{\odot} < 1.0$ and $M_{\odot} < 1.0$ and $4.5 \leqslant M_{\odot} < 2.5$, $2.5 \leqslant M_{\odot} < 1.5$ and $M_{\odot} < 1.5$ mag for Tr 1 and Be 11, respectively. The K-S test indicates that mass segregation has occurred at a confidence level of 99 per cent for Tr 1 and 80 per cent for Be 11. One would like to know whether the existing mass segregation is caused by dynamical evolution or is an imprint of the star formation process.

Dynamical evolution is one of the possible causes for mass segregation. At the time of formation, the cluster may have a uniform spatial stellar mass distribution, which may be modified owing to dynamical evolution of the cluster members. Because of dynamical relaxation, low-mass stars in a cluster may possess the largest random velocities, consequently these will try to occupy a larger volume than the high-mass stars (cf. Mathieu 1985; Mathieu & Latham 1986; McNamara & Sekiguchi 1986). Thus mass segregation develops on the time-scale required to exchange energy between stars of different mass by scattering. The dynamical relaxation time, T_E is the time over which the individual stars exchange energy and their velocity distribution approaches a Maxwellian equilibrium. It is given by

$$T_E = \frac{8.9 \times 10^5 N^{1/2} R_{\rm h}^{3/2}}{\langle m \rangle^{1/2} \log(0.4N)},$$

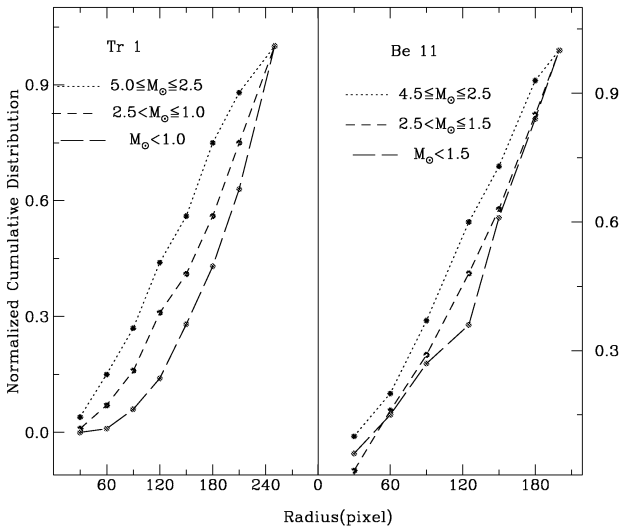

Figure 13. Cumulative radial distribution of stars in different mass ranges for Tr 1 and Be 11.

where N is the number of cluster members, $R_{\rm h}$ is the radius containing half of the cluster mass and $\langle m \rangle$ is the average mass of the cluster stars (cf. Spitzer & Hart 1971). The number of probable MS stars is estimated using the CMDs of the clusters after subtracting the contribution owing to field stars and applying the necessary corrections for the data incompleteness. Owing to our inability to estimate the $R_{\rm h}$ from the present data, we assume that the $R_{\rm h}$ is equal to half of our cluster radius value. The angular values are converted to linear values using the cluster distances, which are derived here. Inclusion of cluster members fainter than the limiting V magnitude will decrease the value of $\langle m \rangle$ and increase the value of N. This will result in higher values of T_E. Hence the T_E values obtained here may be considered as a lower limit.

A comparison of cluster age with its relaxation time indicates that the relaxation time is smaller than the age of the clusters. Thus, we can conclude that the clusters under study are dynamically relaxed. It may be the result of dynamical evolution or an imprint of star formation processes or both.

6 CONCLUSIONS

Physical parameters of the young open star cluster Tr 1 and Be 11 have been derived based on *UBVRI* CCD photometry. Our study leads to the following conclusions.

(i) The radial density profiles of the clusters indicate the existence of clustering. The angular diameter of the clusters Tr 1 and Be 11 are 6.0 and 4.8 arcmin, respectively. The corresponding linear sizes are 4.6 and 3.0 pc, respectively.

(ii) Variable reddening is present within both clusters Tr 1 and Be 11 with a mean value of $E(B-V) = 0.60 \pm 0.05$ and 0.95 ± 0.05 mag, respectively. The interstellar extinction law is normal in the direction of both the clusters. Combining 2MASS data with optical data, we have studied the extinction law in the direction of Be 11. A colour–colour diagram yields a colour excess of $E(J-K) = 0.40 \pm 0.20$ mag and $E(V-K) = 2.20 \pm 0.20$ mag, respectively.

(iii) The distance values are 2.6 ± 0.10 and 2.2 ± 0.10 kpc for clusters Tr 1 and Be 11, respectively. The fitting of the isochrones of Schaller et al. (1992) to the intrinsic CM diagrams indicates an age of 40 ± 10 and 110 ± 10 Myr for Tr 1 and Be 11, respectively.

(iv) The luminosity function of clusters was constructed by subtracting field star contamination determined from neighbouring fields. The luminosity function was transformed into a mass function using the present cluster parameters and the theoretical model given by Schaller et al. (1992). This gives a mass function slope of $x = 1.50 \pm 0.40$ and 1.22 ± 0.24 for Tr 1 and Be 11, respectively. The values of x for Tr 1 and Be 11 thus agree with the Salpeter (1955) value.

(v) Mass segregation, in the sense that massive stars tend to lie near the cluster centre, is observed in both clusters Tr 1 and Be 11. The dynamical relaxation time indicates that both clusters are dynamically relaxed and mass segregation may have occurred owing to dynamical evolution, or be an imprint of star formation or both.

(vi) The present data are unable to identify the members of the clusters unambiguously – for this, precise kinematic observations will be required.

ACKNOWLEDGMENTS

We gratefully acknowledge the useful comments given by the referee J. C. Mermilliod, which improved the paper significantly. We are also grateful to Dr Vijay Mohan for helping in data reduction. Useful

discussions with Dr A. K. Pandey are gratefully acknowledged. This study made use of 2MASS and WEBDA.

REFERENCES

Alcalá J.M., Ferro A.A., 1988, Rev. Mex. Astro. Astrofis, 16, 81
Banks T., Dodd R.J., Sullivan D.J., 1995, MNRAS, 274, 1225
Burki G., 1975, A&A, 43, 37
Caldwell A.R., Cousins A.W.J., Ahlers C.C., Wamelen P. van, Maritz E.J., 1993, SAAO Circ. no 15
Cardelli J.A., Clayton G.C., Mathis J.S., 1989, ApJ, 345, 245
Hawarden T.G., 1971, Observatory, 91, 78
Jackson P.D., Fitzgerald M.P., Moffat A.F.J., 1980, A&AS, 41, 211
Johnson H.L., Morgan W.W., 1953, ApJ, 117, 313
Joshi U.C., Sagar R., 1977, Ap&SS, 48, 225
Kaluzny J., 1992, Acta Astron., 42, 29
Kamp L.W., 1974, A&AS, 16, 1
Landolt A.U., 1992, AJ, 104, 340
Mateo M., 1988, ApJ, 331, 261
Mathieu R.D., 1985, in Goodman J., Hut P., eds, Dynamics of Star Clusters, Vol. 113. D. Reidel, Dordrecht, p. 427
Mathieu R.D., Latham D.W., 1986, AJ, 92, 1364
McCuskey S.W., Houk N., 1964, AJ, 69, 412
McNamara B.J., Sekiguchi K., 1986, ApJ, 310, 613
Mermilliod J.C., 1995, in Egret E., Abrecht M.A., eds, Information and On-line Data in Astronomy. Kulwer, Dordrecht, p. 227
Moitinho A., 2001, A&A, 370, 436
Nilakshi, Sagar R., Pandey A.K., Mohan V., 2002, A&A, 383, 153
Oja T., 1966, Arkiv Astron., 4, 15
Persson S.E., Murphy D.C., Krzeminski W., Roth M., Rieke M.J., 1998, AJ, 116, 2475
Phelps R.L., Janes K., 1993, AJ, 106, 1870
Phelps R.L., Janes K., 1994, ApJS, 90, 31
Sagar R., 1987, MNRAS, 228, 483
Sagar R., 2002, in Grebel E., ed., Proc. IAU Symp. 207, Extragalactic Star Clusters. Astron. Soc. Pac., San Francisco
Sagar R., Joshi U.C., 1979, Ap&SS, 66, 3
Sagar R., Qian, 1990, ApJ, 353, 174
Sagar R., Richtler T., 1991, A&A, 250, 324
Sagar R., Miakutin V.I., Piskunov A.E., Dluzhnevskaia O.B., 1988, MNRAS, 234, 831
Salpeter E.E., 1955, ApJ, 121, 161
Schaller G., Schaerer D., Meynet G., Maeder A., 1992, A&AS, 96, 269
Schmidt-Kaler Th., 1982, in Scaifers K., Voigt H.H., eds, Landolt/Bornstein, Numerical Data and Functional Relationship in Science and Technology, New series, Group VI, Vol. 2b. Springer-Verlag, Berlin, p. 14
Spitzer L., Hart M.H., 1971, ApJ, 164, 399
Steppe H., 1974, A&AS, 15, 91
Stetson P.B., 1987, PASP, 99, 191
Walker A.R., 1985, MNRAS, 213, 889
Walker A.R., 1987, MNRAS, 229, 31
Whittet D.C.B., van Breda I.G., 1980, MNRAS, 192, 467
Yadav R.K.S., Sagar R., 2001, MNRAS, 328, 370

This paper has been typeset from a TEX/LATEX file prepared by the author.